Available online at www.sciencedirect.com
ScienceDirect
Journal of Crystal Growth 297 (2006) 211–222
JOURNAL OF CRYSTAL GROWTH
www.elsevier.com/locate/jcrysgro

Dendrite growth velocity in levitated undercooled nickel melts

O. Funke[a], G. Phanikumar[a,c], P.K. Galenko[a,*], L. Chernova[a], S. Reutzel[a,b], M. Kolbe[a], D.M. Herlach[a]

[a]German Aerospace Center (DLR), Institute of Space Simulation, 51170 Cologne, Germany
[b]Ruhr-University, Institute of Experimental Physics IV, 44780 Bochum, Germany
[c]Department of Metallurgical and Materials Engineering, Indian Institute of Technology Madras, Chennai, India

Received 21 February 2006; accepted 30 August 2006
Communicated by T.F. Kuech
Available online 18 October 2006

Abstract

Model predictions for the dendrite growth velocity at low undercoolings are deviating significantly from experimental data obtained in electromagnetic levitation with a capacitance proximity sensor (CPS) [K. Eckler, D.M. Herlach, Mater. Sci. Eng. A 178 (1994) 159]. In addition to that, previous data sets obtained by different techniques are not in good agreement with each other. For instance, growth velocity data for nickel melts obtained with a high-speed camera system [D.M. Matson, in: Solidification 1998, TMS, Warrendale PA, 1998, p. 233] show higher values at low undercoolings than data obtained with the CPS. Within this work new measurements of dendritic growth velocity in levitated undercooled nickel samples were performed as a function of undercooling ΔT to investigate this discrepancy. Solidification of the undercooled melt was detected at undercooling levels within the range of $30\,\mathrm{K} < \Delta T < 300\,\mathrm{K}$. The new data reveal high accuracy and low scattering. These data are compared with two independent growth velocity data sets and discrepancies are discussed. For verification of the new CPS data dendrite growth velocity was also measured by using a high-speed camera where the morphology of the intersection of the solidification front with the sample surface was investigated. The new experimental data are analyzed within the model of dendrite growth obtained on the basis of Brener's theory [E. Brener, J. Crystal Growth 99 (1990) 165] and the model of dendrite growth with melt convection in a solidifying levitated drop, presently being developed. Special attention is paid to the effects of convection and small amounts of impurities on the growth dynamics at small undercoolings.

PACS: 05.70.Fh; 68.70.+w; 81.10.Aj

Keywords: A1. Dendritic solidification; A1. Electromagnetic levitation; A1. Growth rate; A1. Undercooling

1. Introduction

Since several decades dendritic growth velocities V have been measured during solidification of electromagnetically levitated metal melts. Different techniques have been applied, e.g. the usage of a fast responding photo-double-diode [1,2] or a high-speed camera system [3]. Following the sharp interface model of dendrite growth by Kurz et al. (LGK/LKT model) [4,5], the prediction of dendritic growth velocity V for nickel as a function of undercooling ΔT is in good agreement with experimental data only in the region of medium undercoolings ($100\,\mathrm{K} < \Delta T < 200\,\mathrm{K}$) [2]. However, for low undercoolings ($\Delta T < 100\,\mathrm{K}$) the LGK/LKT model is not able to describe the experimental data: the predicted growth velocity is too low and the discrepancy is actually increasing with decreasing ΔT [2,6].

The present investigation concentrates on the discrepancy occurring especially at low undercoolings. As already suggested [6], convection rolls occur in drops of pure Ni due to stirring of the melt during electromagnetic levitation. The fluid flow direction of convection rolls can be upwards in the vicinity of the surface and downwards in the middle of the

*Corresponding author. Tel.: +49 2203 601 4582; fax: +49 2203 601 2255.
E-mail address: peter.galenko@dlr.de (P.K. Galenko).

0022-0248/$ - see front matter © 2006 Elsevier B.V. All rights reserved.
doi:10.1016/j.jcrysgro.2006.08.045

liquid sample [6–8]. If crystallization is externally initiated at the south pole of the melt, i.e. the bottommost point on the sample surface, the dendrites growing upwards from the nucleation point are experiencing acceleration in their growth dynamics. This is due to the thermal transport in the fluid stream flowing downwards and hence, opposite to the direction of dendrite growth in the middle of the sample.

A modification of the sharp interface model takes into account the effect of forced convective flow caused by electromagnetic stirring [6]. It is shown that this modification leads to an increase of the calculated velocity values. However, the effect of forced convective flow can still not explain the measured data in a satisfying manner [6]. In order to verify the predictions of various theories of dendrite growth, in particular at small undercoolings, high-accuracy measurements are needed. In this article current results of dendrite growth velocity measurements of electromagnetically levitated undercooled Ni melts are presented and compared with results of previous data [2,3]. The use of the high-speed camera system allows a visualization of the solidification morphology at the sample surface as well as the performance of comparative studies of growth velocity measurements by using the CPS technique.

2. Experiments

2.1. Experimental setup

An electromagnetic levitation facility as described elsewhere [9,10] is used to containerless-process the samples and to measure the velocity of dendritic solidification from the undercooled melt. In the setup the sample is levitated from the sample holder due to the conical design of the electromagnetic coil. In this work an electromagnetic coil of a new, non-conical design is applied to the levitation facility leading to an enhanced stability of the sample. A scheme of the experimental setup is sketched in Fig. 1.

The sample is placed on an Al_2O_3 sample holder tube and inserted into the coil which has an inhomogeneous electromagnetic field in its central part. After the beginning of electromagnetic levitation the sample holder is retracted. Within the sample holder a nickel needle which is part of a capacitance controlled electromagnetic oscillator [10] is inserted acting as a sensing trigger. At the time t_1, when the tip of the needle contacts the melt from below, solidification is triggered and the solidification front starts propagating upwards to the north pole of the sample. At the moment of triggering the capacitance of the needle changes by ΔC due to the enlarged surface and the CPS yields a voltage signal $U(t)$, which is recorded by a transient recorder. A small area around the north pole is projected by an optical system on a fast responding photo diode (Siemens SFH206).[1] As soon as the solidification front arrives at the north pole a fast increase in the brightness of the sample $S(t)$ is measured by the photodiode. The detection of this brightness increase at the time t_2 is simultaneously recorded by the transient recorder. During the time span $\Delta t = t_2 - t_1$ the solidification front passes the vertical distance h of the sample from south to north pole. This distance h is measured for the *as-solidified* sample after the experiment. The growth velocity is then evaluated by the relation $V = h/\Delta t$. In a real experiment the location of triggering will not be exactly at the south pole but in the vicinity. If a deviation of up to 1 mm from the south pole is assumed, the true path length travelled by the solidification front deviates from h by ± 0.15 mm. Fig. 2 shows the recorded signals of the CPS and the photo diode for a Ni sample undercooled by $\Delta T = 57$ K prior to solidification. The sample height was $h = 6.5\,\text{mm} \pm 0.15\,\text{mm}$, the measured time span was $\Delta t = 4.31 \times 10^{-3} \pm 5 \times 10^{-5}$ s, resulting in a growth velocity of $V = 1.51 \pm 0.04\,\text{m s}^{-1}$.

2.2. Experimental results

The growth velocity V was measured as a function of undercooling ΔT for six individual Ni samples with a purity of 99.99% and masses of $1.0\,\text{g} \leqslant m \leqslant 1.5\,\text{g}$, corresponding to a diameter of about 6–7 mm. In order to reduce impurities by e.g. oxidation sources during experiment a high-purity gas mixture of 92% Helium 8% Hydrogen (with purity of 99.9990%) was utilized for convective cooling of the levitated melt. The high-frequency generator inducing the alternating current in the levitation coil was operated at constant power output during individual measurements in order to avoid strengthening/weakening of electromagnetic stirring which could cause changes in thermophysical properties of the melt during experiment.

The CPS results of the present work (filled circles) are shown in Fig. 3 in comparison with the previous CPS data obtained by Eckler and Herlach (open squares) [2] and high-speed camera data (open triangles) of Matson [3]. Considering both CPS data sets it is remarkable that the new CPS data show much less scattering than the previously obtained data, which might be attributed to the new coil design. Another two features are prominent: (i) in the region from $65\,\text{K} \leqslant \Delta T \leqslant 180\,\text{K}$ the new CPS data set shows definitely higher growth velocities than the older CPS data, and (ii) fitting a third order polynomial to each set of data reveals a clear difference in the way of velocity increase with increasing undercooling level: going from low to high undercoolings, the fit curves to the camera data [3] and the CPS data of the present investigation show a rather monotonous increase, while for the older CPS data [2] the fit curve shows significant changes in the velocity increase, respectively.

[1] The photo sensitive area of the Siemens SFH206 is seven times larger than that of the Siemens BPX65 used in the experimental CPS setup of Eckler and Herlach [2]. The larger area leads to a more pronounced dampening in the photo diode's signal rise time. Therefore, we used the beginning of the sample's brightness increase for the determination of the time interval ΔT throughout in our investigation, in contrast to Eckler and Herlach, who used the end of the brightness increase.

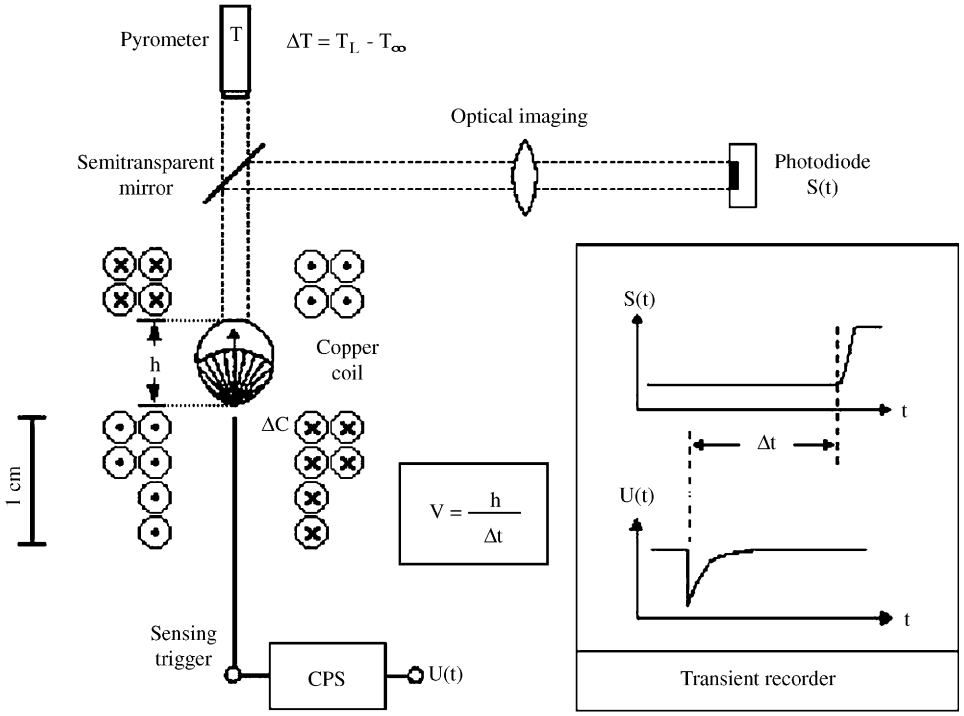

Fig. 1. Experimental setup in the style of Eckler et al. [10] for high-accuracy measurements of the dendrite growth velocity V as a function of undercooling. Deviating from Eckler's setup a newly designed electromagnetic coil is applied. A contactless measurement of the sample's temperature is done with a two-colour pyrometer. The undercooling ΔT is defined as $\Delta T = T_L - T_\infty$, with the liquidus temperature T_L and the actual temperature of the undercooled state T_∞.

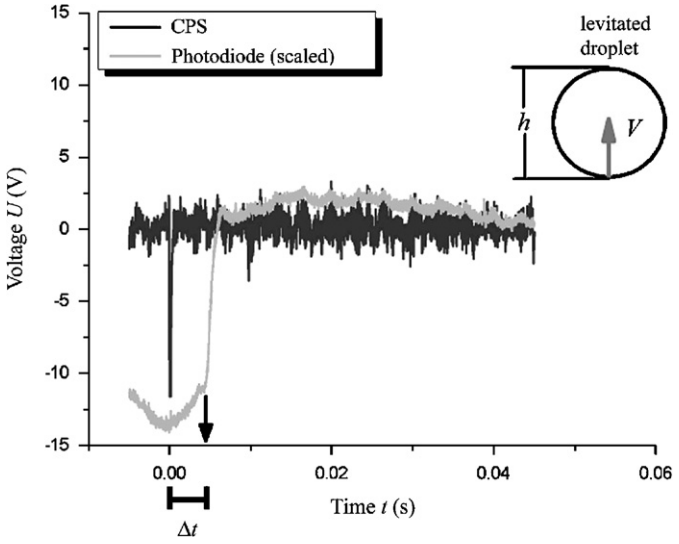

Fig. 2. Typical CPS and photo diode signal from real experiment with the following parameters: $\Delta T = 57\,\mathrm{K}$, $h = 6.5\,\mathrm{mm}$, $\Delta t = 4.31\,\mathrm{ms}$, and $V = 1.51\,\mathrm{ms}^{-1}$. The time span between both signals can be measured very precisely, also the height of the as solidified sample and thus the length of the solidification path. The intensity of the photo diode signal was scaled to overlay with the CPS signal. The arrow indicates the first appearance of the front of recalescence on the top of the droplet.

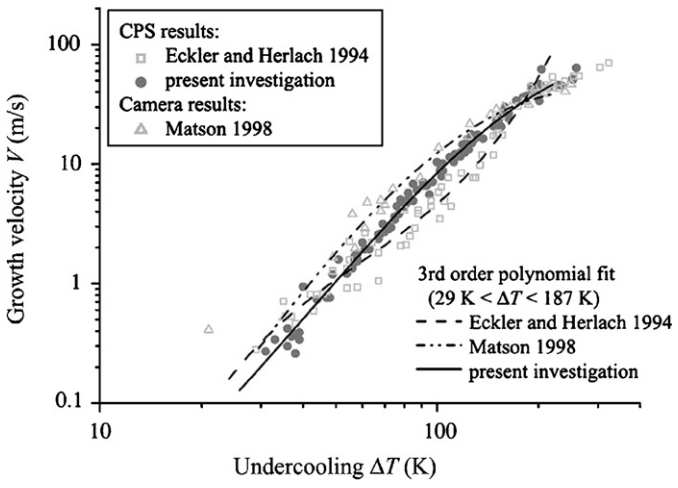

Fig. 3. Comparison of three independent experimental data sets: CPS data of Eckler and Herlach (open squares) [2], high-speed camera data of Matson (open triangles) [3], and the new CPS data (filled circles) of the investigation presented in this article. The new CPS data show less scattering in comparison with the other two data sets. At undercoolings of $\Delta T < 60\,\mathrm{K}$ and $\Delta T > 180\,\mathrm{K}$ both CPS data sets are in good agreement. Within this interval $60\,\mathrm{K} < \Delta T < 180\,\mathrm{K}$ the new data reveal higher velocities than measured by Eckler and Herlach and lower velocities than found by Matson. The new data as well as Matson's data are following a rather smooth curve and reveal a monotonous increase in V, whereas the old CPS data set shows a distinct temperature dependence in the degree of velocity increase with increasing degree of undercooling. The axes are in logarithmic scale.

At $\Delta T \approx 65\,\mathrm{K}$ the deviation in both CPS data sets starts, showing a maximum disagreement at $\Delta T \approx 130\,\mathrm{K}$. At this undercooling the older CPS data show a change in the

velocity versus undercooling relation followed by a stronger increase of $V(\Delta T)$. This increase is definitely steeper than the rather uniform increase that is apparent in the new CPS data set as well as in the camera data. Finally, this steep increase results in a merge of old and new CPS data at an undercooling level $\Delta T^* \approx 180\,\mathrm{K}$. From this point on discrepancies in both data sets are marginal.

The main characteristics of all three data sets under consideration therefore can be summarized as follows:

1. The present CPS data show low scattering and high reproducibility and reveal a rather uniform increase in $V(\Delta T)$ with increasing ΔT.
2. In comparison with the present results the old CPS data set [2] shows a sharp transition to lower velocity increase at $\Delta T^* \approx 180\,\mathrm{K}$.
3. In addition, Matson's results [3] show higher values than the present CPS data for growth velocities below 180 K undercooling level and slightly lower values above 180 K.

For further analysis of dendritic growth kinetics a high-speed camera system (Photron Fastcam Ultima APX) was used to investigate growth dynamics of levitated pure nickel melts at different levels of undercooling. Fig. 4 illustrates changes in the morphology of the advancing solidification front for solidification triggered at $\Delta T = 90\,\mathrm{K}$ (top sequence, Fig. 4(a), only every fifth image is displayed here) and $\Delta T = 140\,\mathrm{K}$ (bottom sequence, Fig. 4(b)). In this presentation the bottom of the sample is directed to the left. The coil hides a small part of the sample bottom/bottom of the sample, while the top of the sample is completely visible. The gap between the upper windings and the bottom windings of the coil has a width of 6.0 mm, while the total height of the sample (measured after its final solidification) was found to be $h = 7.0\,\mathrm{mm}$. The visible sample height in the images is $h' \approx 5.95\,\mathrm{mm}$. Both image sequences in Fig. 4 were taken at a rate of 30000 frames per second (fps), the time Δt for propagating the (visible) distance h' through the sample is $\Delta t = 1.2\,\mathrm{ms}$ (36 individual images) for $\Delta T = 90\,\mathrm{K}$ and $\Delta t = 367\,\mu\mathrm{s}$ (11 individual images) for $\Delta T = 140\,\mathrm{K}$. Calculating from this the growth velocity $V(\Delta T)$ results as follows: $V(90\,\mathrm{K}) = 4.96\,\mathrm{ms}^{-1}$ and $V(140\,\mathrm{K}) = 16.21\,\mathrm{ms}^{-1}$, respectively. Within the assumptions made for the visible sample size these values are in agreement with the new CPS data set.

Regarding the appearance of the solidification front in Fig. 4 a clear difference can be listed. Following Matson's nomenclature as given in Ref. [3], the shape of the solidification front is angular at an undercooling level $\Delta T = 90\,\mathrm{K}$ (Fig. 4(a)). For an undercooling level $\Delta T = 140\,\mathrm{K}$ (Fig. 4(b)), however, the appearance of the solidification front has changed showing a rather smooth (spherical) solidification front (i.e. front of recalescence), which can be approximated by the envelope surrounding the dendrites' tips. For this transition from angular to spherical growth Matson attributed an abrupt change of the slope of the velocity-undercooling curve [3]. The present results cannot confirm this finding. In our studies the transition is not reflected by a dramatic change of the velocity-undercooling curve, see Fig. 3, which shows a smooth and monotonic increase in the respective undercooling range, $90\,\mathrm{K} < \Delta T < 140\,\mathrm{K}$.

A remarkable feature sometimes appearing simultaneously with an angular front is shown in Fig. 5. In the view from the side (Fig. 5(a)) as well as in the top view onto the sample's north pole (Fig. 5(b)) a small bright spot appears in the second image from the left and is continuously growing in the consecutive images. It is interpreted as the recalescence associated with a central dendrite, which appears at the top of the sample. Since the sample is completely visible the time t_1 of the beginning of solidification can be determined precisely. Analogous to the CPS measurements the point of time t_2 is defined as the moment of first appearance of *either* the tip of a central dendrite *or* of the contraction of the solidification front close to the sample's north pole, respectively.

Solidification velocities derived from the high-speed camera observations and of the new CPS results are presented in Fig. 6. Both sets of data are in good

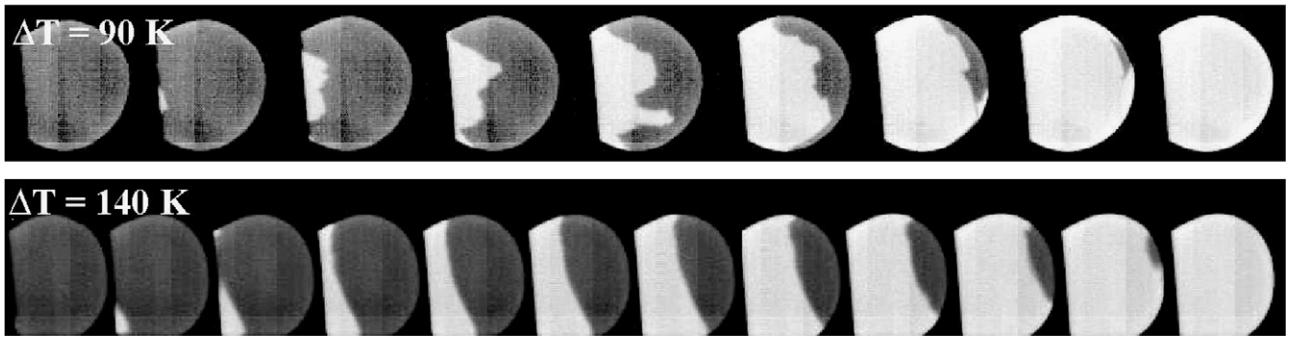

Fig. 4. Visualization of the solidification front intersecting the sample surface: *Top sequence*: solidification triggered at an initial undercooling $\Delta T = 90\,\mathrm{K}$. *Bottom sequence*: solidification triggered at an initial undercooling $\Delta T = 140\,\mathrm{K}$. The solidification front is of angular shape at $\Delta T = 90\,\mathrm{K}$ while at $\Delta T = 140\,\mathrm{K}$ a smooth shape is visible. The images were taken at a rate of 30000 frames per second; in sequence (a) only each fifth image is displayed. For taking advantage of the enhanced horizontal resolution (256 × 128 pixel) the camera was tilted by 90°, the top of the sample is therefore on the right, triggering occurred from the left side at the bottom of the sample, not visible due to partial coverage by the coil.

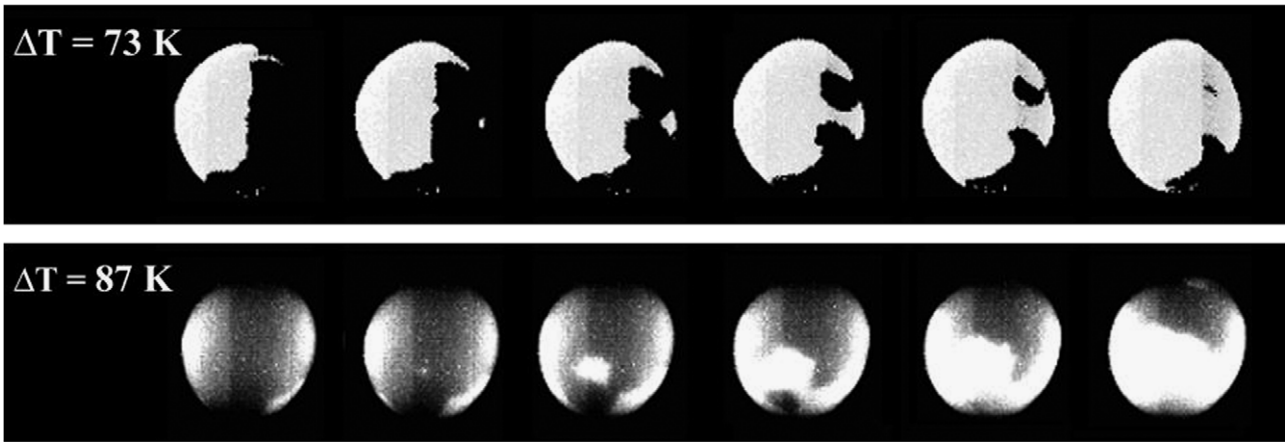

Fig. 5. *Top sequence*: solidification of a Ni sample at an undercooling level $\Delta T = 73\,\mathrm{K}$, viewed from the side. The second depicted frame shows the appearance of a central dendrite on top of the sample, which in this view is to the right. *Bottom sequence*: solidification at an undercooling level $\Delta T = 87\,\mathrm{K}$, view on the top of the sample. Here, the solidification morphology is similar to that in (a) a single dendrite is appearing close to the sample's north pole before the growing side branches have pushed the solidification front to that region. Both examples are recorded at a frame rate of 30.000 frames per second. For visualization purpose the sequences do not show all consecutive frames.

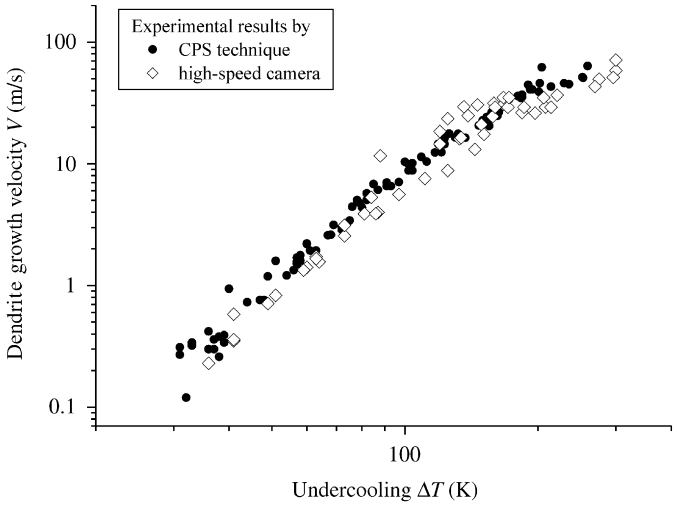

Fig. 6. Verification of the new CPS data compared with data obtained by using a high-speed camera system. The axes are in logarithmic scale.

agreement. However, the camera data tend to agree better to the minimum values of the CPS data for $\Delta T < 100\,\mathrm{K}$. For further interpretations the present data are analyzed in comparison with theoretical model predictions, described in detail in the following section.

3. The model

Electromagnetic levitation exhibits complicated phenomena of interaction of heat transport and electromagnetic fields with the moving solid–liquid interface. For instance, heating and cooling of a droplet, the flow of the induced current, the inclusion of the liquid phase of the droplet into the forced flow due to the Lorentz force caused by the alternating electromagnetic field, and the solidification process itself lead to these complicated phenomena [11].

The problem of the external forced flow imposed on a dendrite growing into an undercooled pure melt has been described theoretically during the past two decades [12–17]. Taking into account the effect of forced convective flow on dendritic growth in a levitated droplet the LGK/LKT model [4,6] as a basic model has been modified and extended [6]. For clarity, the final system of equations of this model is summarized as follows.

First, it is assumed that during the levitation process the dendritic ensemble is growing in such a way that the temperature fields around each of the dendritic tips are not overlapping. Therefore, one may consider the growth of a single dendrite to verify the present model of dendritic growth in comparison with experimental data of solidification obtained in electromagnetic levitation facilities. Second, an axisymmetric parabolic shape of the dendrite tip is considered which has the interface temperature T_I and propagates into the undercooled melt with constant velocity V. The total undercooling $\Delta T = T_\mathrm{L} - T_\infty$ (T_L is the melting temperature) at the dendrite tip consists of the following contributions:

$$\Delta T = \Delta T_\mathrm{T} + \Delta T_\mathrm{R} + \Delta T_\mathrm{K}. \tag{1}$$

Here, ΔT_T is the thermal undercooling, ΔT_R is the undercooling at the curved interface due to the Gibbs–Thomson effect, and ΔT_K is the kinetic undercooling.

The thermal undercooling $\Delta T_\mathrm{T} = T_\mathrm{I} - T_\infty$ (T_∞ is the temperature in the liquid far from the interface) for the removal of latent heat released at the dendrite's tip is described by

$$\Delta T_\mathrm{T} = T_\mathrm{Q} Pe_\mathrm{g} \exp(Pe_\mathrm{g} + Pe_\mathrm{f}) \int_1^\infty \eta^{-1} \times \exp[-\eta Pe_\mathrm{g} + (\ln \eta - \eta) Pe_\mathrm{f}]\, \mathrm{d}\eta, \tag{2}$$

where V and R are the tip velocity and tip radius of the parabolic dendrite, respectively, T_Q is the adiabatic

temperature of solidification defined by $T_Q = Q/c_p$, Q and c_p are the latent heat of solidification and specific heat per unit volume, respectively, $Pe_g = VR/(2a)$ is the thermal Peclet number, $Pe_f = U_0R/(2a)$ is the flow Peclet number, U_0 is the velocity of the uniform forced flow far from the dendrite tip, and a denotes the thermal diffusivity of the liquid.

The flow velocity U_0 in the levitated droplet can be defined from a special consideration of the energy balance for the energies of the electromagnetic field, the gravitational field, and the viscous dissipation. This yields

$$U_0 = \left[\frac{2}{\rho}\left(\rho g R_0 + \frac{B_0^2[1-\exp(-2R_0/\delta)]}{8\pi} + \frac{\rho\mu^2}{2\delta^2}\right)\right]^{1/2}, \quad (3)$$

where g is the modulus of the vector of gravity acceleration, ρ is the density, R_0 is the averaged radius of the droplet, and μ is the dynamic viscosity of the liquid phase. In this case the velocity U_0 included in the thermal undercooling, Eq. (2) as a free parameter becomes now independently defined from Eq. (3) for the electromagnetic levitation process.

The penetration depth δ in Eq. (3) is considered as a skin depth of the surrounding high-frequency magnetic field into the sample and hence, the region where the induced eddy current provides for the heating. The skin depth δ is defined by the electric and magnetic parameters as follows:

$$\delta = \left(\frac{2}{\omega\sigma_R\mu_0}\right)^{1/2}, \quad (4)$$

where σ_R is the electrical conductivity (measured under isothermal conditions), μ_0 is the magnetic permeability, and ω is the frequency of the applied current. As a result, δ can be considered as a skin depth for the alternating magnetic field in the liquid droplet which propagates for a short distance where the magnetic field decays by the exponential law $|B| = B_0 \exp[(r-R_0)/\delta]$. Here, $|B|$ is the modulus of the magnetic induction vector, B_0 is the time averaged value of the magnetic induction, and r is the radial distance within a droplet of radius R_0.

In Eq. (1), the curvature undercooling ΔT_R due to the Gibbs–Thomson effect is described by

$$\Delta T_R = 2\Gamma_0(1 - 15\varepsilon_c \cos 4\theta)/R, \quad (5)$$

where Γ_0 is the capillary constant, ε_c is the parameter of anisotropy of the surface energy, and θ is the angle between the normal to the interface and the direction of growth along the z-axis. The kinetic undercooling ΔT_K which is necessary for the attachment of atoms to the interface is described by

$$\Delta T_K = V/\mu_k, \quad \mu_k = \mu_{k0}(1 - \varepsilon_k \cos 4\theta), \quad (6)$$

where μ_k is the kinetic coefficient for anisotropic dendritic growth, μ_{k0} is the averaged kinetic growth coefficient, and ε_k is the parameter of anisotropy for the growth kinetics. Obviously, at the tip of the axisymmetric dendrite one assumes $\theta = 0$ for Eqs. (5) and (6). Taking into account the notations from Eqs. (1)–(6) one gets the first equation for two variables, i.e. for the dendrite's tip velocity V and dendrite's tip radius R. The second equation is obtained from consideration of the stable dendrite growth mode (the so-called "selection criterion for the dendritic tip"). A special analytical treatment by using a solvability condition gives an expression for dendrite growth with the stable tip [16]

$$R = \frac{\Gamma}{\sigma^* T_Q Pe_g}, \quad (7)$$

with the stability parameter σ^* given by

$$\sigma^* = \sigma_0 \varepsilon_c^{7/4}\left[1 + \chi(Re)\frac{U_0\Gamma}{aT_Q}\right]^{-1}, \quad (8)$$

where σ_0 is a constant, and $Re = U_0R/\mu$ is the Reynolds number. The function $\chi(Re)$ can be found in Ref. [16] (with adaptation of the analytical results to the 3D solution). For computation of the stability parameter σ^* we have chosen the results of phase-field modelling [17] according to $\sigma_0\,\varepsilon_c{}^{7/4}/\sigma^* = 1.675$ for the 3D upstream fluid flow imposed on the scale of a free-growing dendrite.

Three points can be outlined for the suggested system of Eqs. (1)–(8):

First, the selection criterion for the growth mode given by Eqs. (7) and (8) is physically reasonable for relatively small undercoolings, i.e. when the growth direction of the dendrite is dictated by the anisotropy of surface energy and the imposed direction of the liquid flow. Selection criterion for dendritic growth under imposed forced flow and in a presence of both anisotropies of surface energy and atomic kinetics is not derived so far.

Second, the obtained system of Eqs. (1)–(8) can be resolved regarding two variables, i.e. the velocity V and tip radius R of the dendrite for a given undercooling ΔT. The system of equations gives a partial limit: in a stagnant undercooled melt, $U_0 = 0$, for the isotropic surface energy and growth kinetics, $\varepsilon_c = 0$ and $\varepsilon_k = 0$, and with application of the marginal stability hypothesis instead of the solvability condition, Eq. (7), solidification is described by the LGK/LKT model [4,5].

Third, Eq. (3) assumes some uniform velocity of the flow inside the droplet. However, alternating electromagnetic forces acting effectively within the penetration depth δ and the surface tension of the droplet result in a non-uniform distribution of the forced flow velocity. In the liquid state, the 3D levitated droplet is divided into two parts in which the melt might be involved in induced forced stirring [18–20].

The question about simultaneous evolution of convective rolls and solidification patterns inside the droplet still remains open (from both computational and experimental points of view). In the present work we observed that the appearance of the solidification front (front of recalescence) is normally more pronounced and developed at the central part of the droplet resulting in the formation of a central dendrite which can be detected by the high-speed video signal (see Fig. 5). One possible scheme of convective rolls inside the droplet during dendritic solidification was already suggested earlier [6]. The evolution of convective patterns leads to an enhancement of dendritic growth in the

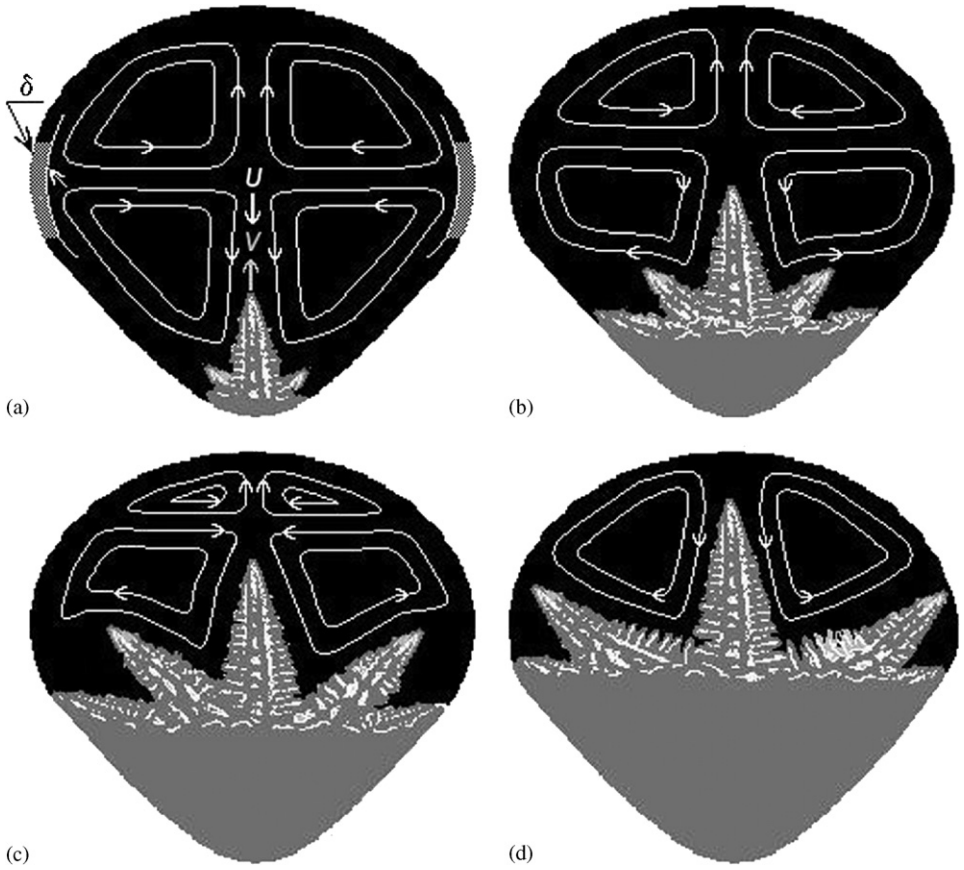

Fig. 7. Schematic draw of the evolution of convective rolls inside a remaining liquid during the dendritic solidification of a droplet. V is the dendrite growth velocity, and U is the flow velocity in the vicinity of the dendritic tip, δ is the penetration depth of the alternating electromagnetic force which involves the metallic liquid in a forced stirring: (a) a view of convective rolls immediately after triggering solidification from the bottom of the droplet; (b) influence of convective rolls of both types (directed opposite to the growth direction and directed along the dendrite growth direction) on the dendrite growth; (c) gradual degeneration of the convective rolls opposite directed to the growth direction; (d) dendrite growth and the stream lines of the flow at some pre-final stage of solidification of the droplet: The flow still has an opposite direction to the dendrite growth direction.

central part of a droplet. This causes the formation of a central dendrite at moderate undercooling levels like depicted schematically in Fig. 7. Immediately after the triggering, the flow inside the droplet is divided into two parts: a convective flow opposite to the dendrite growth direction in the bottom part, enhancing the growth velocity V (Fig. 7(a)), and convective flow parallel to dendrite growth in the upper part. During the dendritic growth, the stream lines may gradually disappear in the top part of the droplet nearby to its north pole (Fig. 7(b) and (c)). At some final stages, the top patterns completely disappear so that the flow with the down-stream velocity U remains still enhancing the dendrite's velocity V (Fig. 7(d)). Therefore, assuming such a scheme in the present model, one may use some uniform flow velocity near the steady-state dendritic tip growing at a given undercooling.

4. Discussion

4.1. Discrepancy between experimental data sets

The new CPS data lie between the values of the other two data sets considered here: at undercooling levels below 180 K the growth velocity of the new CPS data set is deviating from the data of Eckler and Herlach [2] to *higher values*, while compared to Matson's data [3] the new data show *lower values*, Fig. 3. The dependence of the growth velocity on undercooling level derived from the previous CPS data shows an abrupt change in the slope of the velocity at $\Delta T \approx 180$ K. Such a change is not apparent in the current results, neither in the camera data nor in the new CPS data set. By comparison of all individual data sets it becomes obvious that the new CPS data show the lowest scattering, while the older CPS data show a relatively high degree of scattering.

For pure Ni theory predicts a rather uniform increase in growth velocity with increasing undercooling (see Fig. 10), which is the case for Matson's data as well as for our new data. The change in the velocity versus undercooling relation in the older CPS data set might hint to the presence of small amounts of impurities in the individual samples used in that investigation. As it has been shown by Eckler et al. [21] small amounts of impurities have a non-negligible influence on the dendrite growth velocity, leading either to an enhancement or a reduction of V depending on the concentration. Also, a pronounced velocity versus

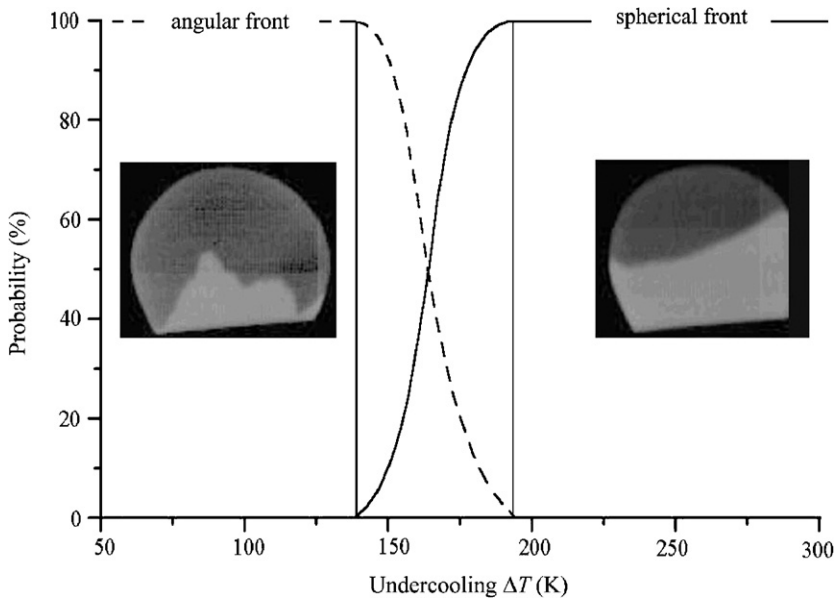

Fig. 8. Schematic presentation of the probability to observe an angular or a spherical front of recalescence at a given undercooling. For intermediate undercooling levels $140\,K < \Delta T < 180\,K$ both, angular front and spherical front have been observed.

undercooling dependence resulting in a "*distinct kink*" at intermediate undercoolings was a result of model calculations by these authors for levitated dilute Ni-C melts.

It can be also noted that, using high-speed camera, Matson [3] observed a transition from angular to spherical shape of the front of recalescence as shown in Fig. 4. He related this transition to the abrupt change in the velocity, which has been found in his measurements for the undercooling of $\Delta T = 160\,K$. He claimed that above this critical undercooling the solidification in undercooled nickel melts proceeds with the spherical shape of the front of recalescence. Our investigation, however, provided a different result. Using a high-speed camera, we collected 52 camera visualizations of solidifying levitated nickel drops in a region from 36 to 300 K of undercooling. We found a region of undercooling (approx. from 140 up to 180 K) in which a gradual transition from angular front to spherical front has been observed. The result is summarized in Fig. 8 where the probability to observe a given solidifying shape is depicted over the given undercooling. Moreover, this gradual transition to the spherical solidification front is found in the region of a smooth dendrite velocity versus undercooling relationship. Therefore, one may conclude that the transition to a smooth front (a) occurs gradually in a range of undercoolings, and (b) does not lead to the sharp break point in the velocity–undercooling relationship.

Regarding the purity of the investigated nickel samples, we analyzed the samples used for the old and the new CPS measurements. Particularly, a detailed metallographical analysis has been made for all samples presently processed and the samples previously processed by Eckler and Herlach [2]. Totally, the samples which solidified in the range of $34\,K < \Delta T < 164\,K$ have been analyzed. As a result the presently processed samples do not exhibit a visible dendritic microstructure after chemical etching. On the contrary, chemical etching revealed the dendritic microstructure in the samples previously processed by Eckler and Herlach, independent of the level of undercooling. This clear difference in the etched microstructures of the samples is visible in Fig. 9. Due to the fact that the dendritic structure can be visualized and identified upon chemical etching only in alloys but not in a pure system, it is concluded that the purity of the samples previously processed by Eckler and Herlach was essentially lower than it is the case for the current investigation. That is why experimental data of Eckler and Herlach are exhibiting the behavior consistent with the behavior of an alloy system. In addition, chemical analyses of the samples used for our current investigation were performed.[2] The results on average for suspected constituents are given in Table 1. It can be noted that due to the usage of a HeH_2-gas mixture as a protective atmosphere and for the sample cooling, the amount of O_2 has decreased during experiment by a factor of approximately two while the content of H_2 has increased by a factor of about five. Note that the overall purity of the sample has become better during experiment. Therefore, one may conclude from the chemical analysis summarized in Table 1 that (i) the highest amount of impurities was found for carbon, (ii) the purity of the samples increased during electromagnetic levitation, and (iii) the overall amount of impurities on average was approximately a total of 0.01 at.%. Presumably, the low level of impurities

[2]For determination of Fe, Co, and Si optical emission spectrometry has been used. Determination of H_2, O_2, and N_2 has been made by gas-chromatography. For determination of C, a combustion method with infra-red spectrometry has been used. The "IME—Metallurgische Prozesstechnik und Metallrecycling, Institut und Lehrstuhl der RWTH Aachen" was chosen for doing the chemical analysis of our samples.

in the presently processed samples accounts for the smooth velocity–undercooling relationship with lowest scattering of all considered data sets (see Fig. 2).

Controlled small amounts of impurities can drastically influence the dendrite growth velocity of nickel dendrites [22,23]. Recent investigations revealed the influence of controlled additions of very small amounts of impurities on the growth velocity characteristics of nickel. The results show that impurities of approximately 0.1 at% slightly enhance the growth velocity, while amounts of about 0.5 at% already reduce the growth velocity clearly [24]. Accompanying model calculations also reveal that impurities affect the pure system for amounts >0.01 at%. This might explain the differences in the available data sets for pure nickel and the different degree of scattering/reproducibility of all data. Recently, results of numerical modelling on the influence of small amounts of impurities on the growth velocity have been published separately [25]. Particularly, using the results of a phase-field model, it was shown that forced convective flow enhances the growth velocity in the range of small undercoolings where the dendrite growth velocity is comparable to the velocity of the flow. Using a sharp interface model it was additionally shown that even small amounts of impurity on the level of 0.01 at% may lead to an enhancement of the dendrite growth velocity in the range of small and intermediate undercoolings. The solute effect, however, exhibits a different temperature characteristic than the transport effect by fluid flow, which allows discriminating between both effects by investigating the growth velocity as a function of undercooling.

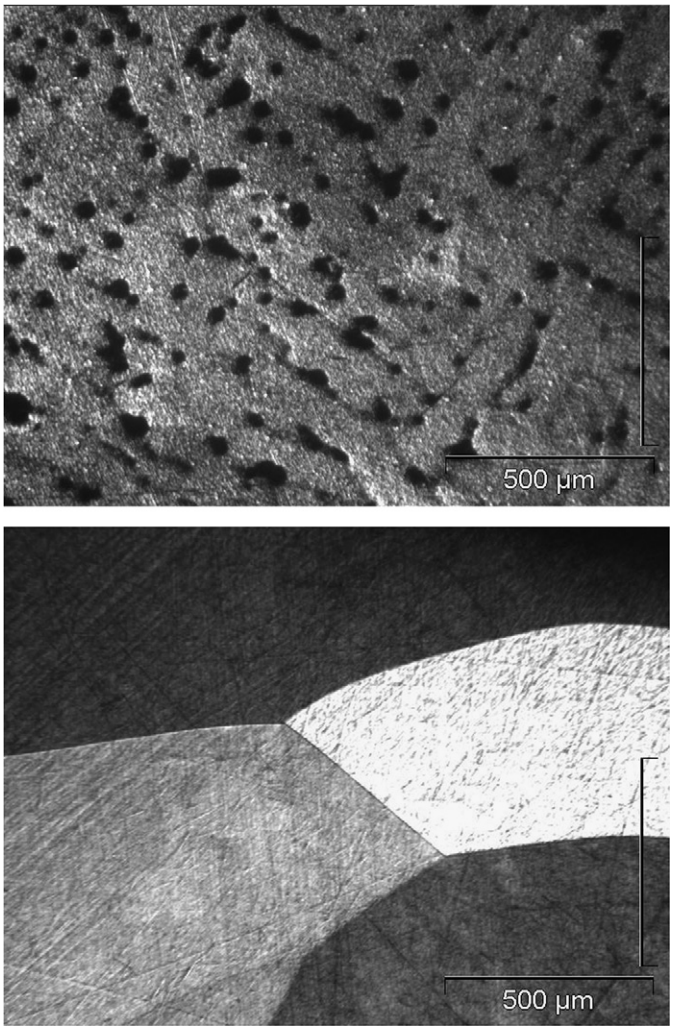

Fig. 9. Typical final microstructure of nickel samples taken from droplets originally used in Ref. [2] (upper picture, $\Delta T = 123$ K) and from droplets used in the present work (lower picture, $\Delta T = 65$ K) for measurements of dendrite growth velocity.

4.2. Deviation of model predictions from experimental data

Previously, it was shown [6] that the inclusion of a forced convective flow into the model of dendritic growth gives a partial satisfactory description of the experimental data of Eckler et al. [2,10] on the solidification of levitated droplets at small undercoolings. In this work the new experimental results of dendritic growth velocity are compared, firstly, with the predictions of Brener's theory [26,27], which does not take into account fluid flow effects and, secondly, with the predictions of the present model, Eqs. (1)–(8).

The analyses of Brener [26,27] and Brener and Melnikov [28] show that for a pure system solidifying at a high undercooling level the anisotropy of kinetics may play a crucial role in the selection of the dendritic growth mode. These analyses are based on the model which takes into account both anisotropies of surface energy and of growth kinetics with parameters of anisotropy ε_c and ε_k [26–28] but no fluid flow (i.e., $U_0 = 0$). The selection criterion presented in this work by Eqs. (7) and (8) takes into account finite forced fluid flow but only includes anisotropy of surface energy. It is due to the fact that stability analysis of dendritic growth with additional fluid flow has only been done with anisotropy of surface energy so far.

Table 1
Outcome of chemical analysis of sample purity

Ni	O_2 (ppm)	H_2 (ppm)	C (ppm)	Si (ppm)	Fe (ppm)	Co (ppm)	Total (ppm) (at%)
Unprocessed	19.2	0.75	56	18	4	2	99.95 (0.009995)
Processed	10.4	3.86	49	10	3	3	79.26 (0.007926)
Average	14.8	2.305	52.5	14	3.5	2.5	89.61 (0.0089.61)

N_2 was below the detection limit of 5 ppm.

For the whole model (Eqs. (1)–(8)) the parameters of anisotropy ε_c and ε_k are taken from data of atomistic simulations of Hoyt et al. [29,30], which have been linked recently with phase-field simulations of Bragard et al. [31] for the analysis of dendritic growth over a wide range of undercoolings. It is remarkable to note that the values for the atomic kinetics given by atomistic simulations [29] are by approximately 4–5 times lower than predicted by the collision-limited theory of Coriell and Turnbull [32] for the advancing interface. Those values are well compared with the values found from previous molecular-dynamic simulation data of Broughton et al. [33]. Concerning the kinetics of rapid dendritic growth of nickel based alloys, Galenko and Danilov [34] showed that a satisfying fit to experimental data is only obtained, if the crystal growth kinetics is regarded by a factor of 5 less than predicted by the theory of collision-limited growth. These outcomes [29,33,34] might be explained due to more complicated behavior of the atomic ensemble fluctuations around the interface leading to slower kinetics in comparison with the ideal situation considered by the collision-limited theory. For the current model of pure nickel solidification material parameters are given in Table 2.

As can be seen from Fig. 10 Brener's theory without convection [27] is clearly in disagreement with the new CPS data at small undercoolings $\Delta T < 100\,\mathrm{K}$, while its predictions agree rather well to the experimental data at higher undercoolings $\Delta T > 150\,\mathrm{K}$. This confirms the idea that forced convection may enhance the dendrite growth velocity at small undercoolings [6] and shows the essential role of anisotropy of the growth kinetics at higher undercoolings.

Including convective flow by Eqs. (1)–(8) the dendrite velocity is enhanced which leads to a partial agreement with experimental data at small undercoolings $\Delta T < 100\,\mathrm{K}$ when the flow velocity is $U_0 = 1.4\,\mathrm{m\,s^{-1}}$ as one of the limiting speeds for the established assumptions of the present model for the forced flow in the laminar regime. This effect of forced flow on dendritic growth is shown by the curves 2 and 3 in Fig. 10. Note that without anisotropy of kinetics ($\varepsilon_k = 0$) and with the averaged kinetic coefficient $\mu_{k0} = 0.45\,\mathrm{m\,s^{-1}\,K^{-1}}$ [29,31] the velocity versus undercooling relation given by curve 3 deviates significantly from the experimental data at medium and high undercoolings ($\Delta T > 100\,\mathrm{K}$). For the case of the ideal collision-limited growth [32] with the averaged kinetic coefficient $\mu_{k0} = 1.2\,\mathrm{m\,s^{-1}\,K^{-1}}$ the experimental data might be described in a satisfactory manner within the medium range $100\,\mathrm{K} < \Delta T < 180\,\mathrm{K}$ (see also the outcomes in Ref. [6]). However, as it is known from theory (see Ref. [28] and references therein) dendritic growth does not occur without crystalline anisotropy, especially, at high undercoolings where the role of anisotropy of surface energy vanishes. Therefore, as it is shown by application of Brener's theory [27] (see curve 1 in Fig. 10), the effect of forced flow on dendritic growth is negligible at medium and high undercoolings and dendrite growth velocity is enhancing due to the presence of kinetic anisotropy. Details of modelling results taking into account the effect of convection as well as both, the anisotropies of surface energy and the anisotropy of kinetics, are summarized elsewhere [25].

Table 2
Material parameters of pure Nickel and characteristics of the electromagnetic facility used in calculations

Parameter	Notion	Numerical value	Reference
Melting temperature	T_L	1727 (K)	[35]
Latent heat of solidification	Q	8.113×10^9 (J/m^3)	[36]
Specific heat	c_p	1.939×10^7 (J/m^3/K)	[36]
Density	ρ	8.1×10^3 (kg/m^3)	[37]
Dynamic viscosity	μ	4.3×10^{-3} (Pa s)	Present work
Thermal diffusivity	a	1.2×10^{-5} (m^2/s)	[37]
Capillary constant	Γ_0	3.4×10^{-7} (K m)	Present work
Angle between the normal to the interface and the dendrite growth direction	θ	0 (deg)	Present work
Parameter of anisotropy of surface energy	ε_c	1.8×10^{-2} (–)	[30,31]

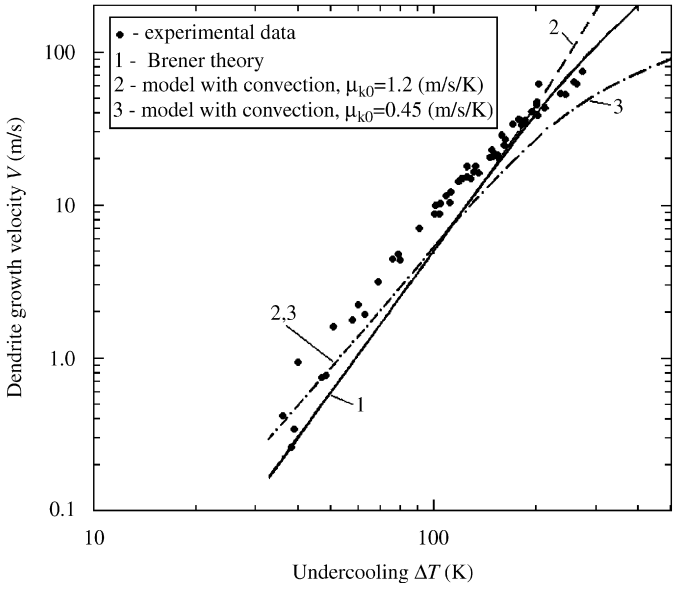

Fig. 10. Model predictions of dendrite tip growth in comparison with the experimental data for pure Ni. The solid line 1 shows the effect of anisotropy of kinetics predicted by the analytical theory of Brener [27]. Predictions of the present model are given by the dashed line and the dashed-dotted line which represent the effect of convective flow with different averaged kinetic coefficients. The velocity U_0 of the upstream flow imposed on the dendrite (curves 2 and 3) has been calculated from Eqs. (3) and (4) to be $1.4\,\mathrm{m\,s^{-1}}$. The axes are in logarithmic scale.

5. Conclusions

Accurate new measurements of dendrite growth velocity as a function of undercooling were performed for pure nickel samples by usage of CPS technique and high-speed camera technique. The new data cover the range of undercoolings from $30\,K < \Delta T < 300\,K$ and show low scattering. We compare the new data with two independent experimental data sets obtained by applying different techniques. Discrepancies are found among all three experimental data sets concerning the velocity values as well as the character of the velocity increase with increasing undercooling.

Our data set shows a smooth velocity-undercooling relationship with lowest scattering of all three considered sets of data (see Fig. 3). Small amounts of impurities influencing the dendrite growth velocity are supposed to explain these discrepancies. Chemical analyses of the samples used in the present investigation show that the amount of impurities in those samples is about 0.01 at.% on average, giving an explanation why the data show very low scattering although the complete data set consists of measurements of six individual samples with different masses. Due to the improved accuracy of the new data set the opportunity is offered to model the dendrite growth velocity as a function of undercooling in a more reliable way. In order to investigate the influence of added controlled amounts of impurities measurements were performed, which show that, indeed, this influence has a non-negligible effect even for amounts of the order of 0.1 at.%, transferring a ''pure'' system to a very dilute binary or even multi-component alloy. These results are published elsewhere [25].

The investigation of the solidification morphology with the high-speed camera system reveals that the change from an angular front to a spherical front cannot be attributed to an existing sharp break point like the critical undercooling. Below $\Delta T < 140\,K$ the angular front has been observed, above $\Delta T > 180\,K$ the spherical front occurs. In a region of $140\,K < \Delta T < 180\,K$ both angular front and spherical front have both been observed.

Concerning the discrepancy among all considered experimental results and model predictions a modification of the standard model of dendrite growth is suggested taking into account the effect of forced convective flow during electromagnetic levitation. This leads to a better description of the dendrite growth velocity, if the speed of the convective flow is comparable to or larger than the dendrite growth velocity. However, discrepancies are still remaining with the experimental data. At medium undercoolings the effect of forced convective flow becomes smaller and vanishes at high undercoolings. In this region the dendrite growth velocity is described by Brener's model, which adopts anisotropy of dendritic growth kinetics.

Acknowledgments

The authors thank Efim Brener, Klaus Eckler, Dirk Holland-Moritz, and Martin Kratz for useful exchanges and valuable discussions, Christoph Ditsche for assistance during the camera observations. Financial support of this work by German Research Foundation (DFG—Deutsche Forschungsgemeinschaft) under the project no. HE 1601/13 and by European Space Agency within the Microgravity Application Programme 'NEQUISOL' is gratefully acknowledged.

References

[1] E. Schleip, R. Willnecker, D.M. Herlach, G.P. Goerler, Mater. Sci. Eng. 98 (1988) 39.
[2] K. Eckler, D.M. Herlach, Mater. Sci. Eng. A 178 (1994) 159.
[3] D.M. Matson, in: S.P. Marsh, J.A. Dantzig, R. Trivedi, W. Hofmeister, M.G. Chu, E.J. Lavernia, J.-H. Chun (Eds.), Solidification 1998, TMS, Warrendale, PA, 1998, p. 233.
[4] J. Lipton, M.E. Glicksman, W. Kurz, Mater. Sci. Eng. 65 (1984) 57; J. Lipton, M.E. Glicksman, W. Kurz, Metal. Trans. 18A (1987) 341.
[5] J. Lipton, W. Kurz, R. Trivedi, Acta Metall. 35 (1987) 957.
[6] P.K. Galenko, O. Funke, J. Wang, D.M. Herlach, Mater. Sci. Eng. A 375–377 (2004) 488.
[7] J.A. Shercliff, J. Fluid Mech. 91 (2) (1979) 231.
[8] B.Q. Li, Int. J. Eng. Sci. 32 (1994) 45.
[9] D.M. Herlach, R. Willnecker, F. Gillessen, In: Proceedings of Fifth European Symposium on Materials Science under Microgravity, ESA SP-2 22, European Space Agency, Noordwijk, The Netherlands, 1985, p. 399.
[10] K. Eckler, M. Kratz, I. Egry, Rev. Sci. Instrum. 64 (9) (1993) 2639.
[11] D.M. Herlach, Annu. Rev. Mater. Sci. 21 (1991) 23; D.M. Herlach, Mater. Sci. Eng. R 12 (1994) 177; D.M. Herlach, Mater. Sci. Eng. A 226–228 (1997) 348; D.M. Herlach, J. Phys: Condens. Matter 13 (2001) 7737.
[12] M. Ben-Amar, Ph. Bouisou, P. Pelce, J. Crystal Growth 92 (1988) 97.
[13] Ph. Bouisou, B. Perrin, P. Tabeling, Phys. Rev. A 40 (1989) 509.
[14] V. Emsellem, P. Tabeling, J. Crystal Growth 92 (1995) 258.
[15] X. Tong, C. Beckermann, A. Karma, Q. Li, Phys. Rev. E 63 (2001) 061601.
[16] Ph. Bouisou, P. Pelce, Phys. Rev. A 40 (1989) 6673.
[17] J.-H. Jeong, N. Goldenfeld, J.A. Danzig, Phys. Rev. E 64 (2001) 041602.
[18] J.-H. Zong, B. Li, J. Szekely, Acta Astronautica 26 (1992) 435.
[19] V. Bojarevics, K. Pericleous, ISIJ Int. 43 (2003) 890.
[20] R.W. Hyers, D.M. Matson, K.F. Kelton, J.R Rogers, in: Proceedings of the Microgravity Transport Processes in Fluid, Thermal, Biological and Materials Sciences III, Davos, CH, September 14–19, 2003.
[21] K. Eckler, D.M. Herlach, R.G. Hamerton, A.L. Greer, Mater. Sci. Eng. A 133 (1991) 730.
[22] K. Eckler, R.F. Cochrane, D.M. Herlach, B. Feuerbacher, M. Jurisch, Phys. Rev. B 45 (1992) 5019.
[23] C.B. Arnold, M. Aziz, M. Schwarz, D.M. Herlach, Phys. Rev. B 59 (1999) 334.
[24] P.K. Galenko, G. Phanikumar, O. Funke, L. Chernova, S. Reutzel, M. Kolbe, D.M. Herlach, Mater. Sci. Eng. A, in press, doi:10.1016/j.msea.2006.02.435.
[25] P.K. Galenko, D.M. Herlach, G. Phanikumar, O. Funke, in: P. Vincenzini, A. Lami, F. Zerbetto (Eds.), Computational Modeling and Simulation of Materials III. Part B, Techna Group, Faenza, Italy, 2004, p. 565; P.K. Galenko, D.M. Herlach, G. Phanikumar, O. Funke, in: D.M.

Herlach (Ed.), Solidification and Crystallization, Wiley-VCH, Weinheim, 2004, p. 52.
[26] E. Brener, Zh. Eksp, Teor. Fiz 97 (7) (1989) 237.
[27] E. Brener, J. Crystal Growth 99 (1990) 165.
[28] E. Brener, V.I. Melnikov, Adv. Phys. 40 (1991) 53.
[29] J.J. Hoyt, B. Sadigh, M. Asta, S.M. Foiles, Acta Mater. 47 (1999) 3181.
[30] J.J. Hoyt, M. Asta, A. Karma, Phys. Rev. Lett. 86 (2001) 5530.
[31] J. Bragard, A. Karma, Y.H. Lee, M. Plapp, Interface Sci. 10 (2–3) (2002) 121.
[32] S.R. Coriell, D. Turnbull, Acta Metall. 30 (1982) 2135.
[33] J.Q. Broughton, G.H. Gilmer, K.A. Jackson, Phys. Rev. Lett. 49 (1982) 1496.
[34] P.K. Galenko, D.A. Danilov, Phys. Lett. A 235 (1997) 271; P.K. Galenko, D.A. Danilov, J. Crystal Growth 197 (1999) 992.
[35] R. Hultgren, P.D. Desai, D.T. Hawkins, M. Gleiser, K.K. Kelley, D. Wagman, Selected Values of the Thermodynamic Properties of the Elements, ASM, Metals Park, OH, 1973.
[36] M. Barth, F. Joo, B. Wei, D.M. Herlach, J. Non-crystalline Solids 156–158 (1993) 398.
[37] K. Eckler, Dendritisches Wachstum in unterkühlten Metallschmelzen, Ph.D. Thesis, Ruhr-Universität Bochum, 1992.